Journal of Solution Chemistry
https://doi.org/10.1007/s10953-023-01354-4

Study of Thermodynamic and Rheological Properties of Sensitive Polymeric Nanoparticles as a Possible Application in the Oil Industry

Lazaro Ruiz-Virgen[1] · Miguel Angel Hernández-Martínez[1] · Gabriela Martínez-Mejía[1] · Rubén Caro-Briones[2] · José Manuel del Río[3] · Mónica Corea[1]

Received: 27 March 2023 / Accepted: 1 December 2023

Abstract
pH and thermo-sensitive polymeric nanoparticles with different morphology were synthesized by means of emulsion polymerization techniques. The materials were characterized by gravimetric techniques, dynamic light scattering (DLS), electrophoresis, Fourier transform infrared spectroscopy (FT-IR), scanning electron microscopy (SEM) and X-Ray diffraction (XRD). The specific volumetric thermodynamic properties were calculated from density (ρ) and sound velocity (u) measurement and they are influenced by the proportions and location of the functional groups in the polymeric particles and the temperature. Rheological properties were also measured, observing that polymeric materials were a non-Newtonian and pseudo-plastic behavior because of they have a decrement in viscosity (η) values as the shear rate rises ($\dot{\gamma}$). In addition, to try to elucidate the behavior that the materials could have with calcite rock in the oil reservoirs, the materials were treated with $CaCl_2$, and changes in the average particle size, colloidal stability and conformation of polymeric chains were observed. The obtained results show that the synthesized polymeric particles could be applied as a possible dosing agent in the interaction with calcium ions (Ca^{2+}) in the calcite rock for petrol industry.

Keywords Polymers · Emulsion polymerization · pH and thermos-sensitive nanoparticles · Acid stimulation

✉ José Manuel del Río
jmdelriogarcia@gmail.com; jdelriog@ipn.mx

✉ Mónica Corea
mcoreat@yahoo.com.mx; mcorea@ipn.mx

[1] Laboratorio de Investigación en Polímeros y Nanomateriales, ESIQIE, Instituto Politécnico Nacional, Av. Luis Enrique Erro S/N, Unidad Profesional Adolfo López Mateos, Zacatenco, Alcaldía Gustavo A. Madero, C.P. 07738 Ciudad de México, México

[2] Posgrado en Ciencias en Metalurgia y Materiales, ESIQIE, Instituto Politécnico Nacional, Av. Luis Enrique Erro S/N, Unidad Profesional Adolfo López Mateos, Zacatenco, Alcaldía Gustavo A. Madero, C.P. 07738 Ciudad de México, México

[3] Escuela Superior de Ingeniería Mecánica y Eléctrica, Unidad Zacatenco, Instituto Politécnico Nacional, Av. Luis Enrique Erro S/N, Unidad Profesional Adolfo López Mateos, Zacatenco, Alcaldía Gustavo A. Madero, C.P. 07738 Ciudad de México, México

Published online: 14 February 2024

1 Introduction

A technique commonly used to improve productivity of oil yield is the acidizing [1]. This process can be classified into three types: acid washing, acid fracturing and matrix acidizing or matrix stimulation [1]. In the latest process, a chemical fluid (acid) with specific properties is injected inside the targeted formation at a pressure less than rock breakdown pressure to dissolve some precipitation around the wellbore and create tiny holes (wormholes) [2, 3]. The process of acid stimulation involves mass transfer, changes of concentration and temperature as a function of time in all parts of the reservoir, while a considerable change in porosity and permeability occur mainly because the dissolution of the hosting rock [4].

An efficient acidizing process depends on wormhole pattern and factors as acid properties, injection rate, wellborn formation properties and the natural fractures [5]. The created wormholes play an important role facilitating the hydrocarbons flow from the reservoir to the wellbore [6].

The acid treatment is used in carbonate reservoirs [6] where carbonate acidizing reduces the formation damage, due to drilling or completion operations and improves the connectivity between the wellbore and reservoir. [7] For this purpose, hydrochloric acid is the main fluid used because its high-dissolving power mainly in calcite ($CaCO_3$) and dolomite ($CaMg([CO_3])_2$), low price and the solubility of formed reaction products ($CaCl_2$ and $MgCl_2$) in the acid dissolution [7–10]. Two factors can limit its use: (i) the high reaction rate and (ii) the severe corrosion of the facilities [11]. For this reason, some stimulation fluids have been developed to solve these problems. For example, HCl - organic acids mixture, HCl- polymers, foamed-HCl, viscoelastic surfactant-based acids, organic acids (formic, lactic and acetic) and emulsified acids [2].

Recently, nanoemulsiones have emerged as attractive colloidal systems with superior properties to the conventional emulsions (i.e. macroemulsions) in areas as biomedical, pharmaceutical, agriculture, textiles, building technology, surface coatings, artificial muscles, catalyst, cosmetics, food, electronics and oil field industry [12–17]. The success of nanoemulsions for oilfield applications will primarily depend of interfacial activity, droplet size, electrophoretic mobility and stability [17].

A new material has been developed to control the acidizing process is the nanoparticles of smart polymers. The smart polymers can undergo reversible or irreversible structural changes as consequence of their physical and chemical properties, when they are submitted to external stimuli such as: ion concentration, light, mechanical force, electricity, magnetism, sound field, and added characteristic substances (ions, bioactive molecules, etc.), pH and temperature [18].

For oil field applications, the smart polymers nanoparticles can be activated changing their surface in response to external stimuli as temperature and pH [19, 20]. The pH-sensitive polymers usually consist of some acid-basic groups such as carboxyl groups, amino groups, imine bonds, hydrazine bonds, among others. The pH changes cause a degree of ionization or hydrolysis of acid-base groups inducing changes in charge, swelling, osmotic pressure, among others [18]. Some monomers that allow a pH change in the polymer structure are the derivatives of acrylic acid. These groups tend to donate protons and acquire negative charge in the presence of specific charge and pH conditions. These polymers suffer swelling, shrinking or conformational changes by the interchange of counter ions from the external environment [21].

Now, the temperature sensitive polymers have a characteristic temperature known as volume phase transition temperature (VPTT) [21]. Above or below of this temperature, the heat-sensitive polymer undergoes a phase transition in solution. There are two types of conversion. The first one is when the polymer is below to certain temperature and shows solubility in water. This is known as lower critical solution temperature (LCST). On the other hand, when the polymer is above a certain temperature, the polymer becomes water soluble. This is known as upper critical solution temperature (UCST) [18]. That means that the solution temperature determines whether a polymeric chain is likely to interact with another polymeric chain or with the medium [22].

The smart polymeric nanoparticles could improve the oil recovery if they are used appropriately [23]. If the polymer nanoparticles are to be applied in oil and gas field scale, they should have the ability to be transported long distance in the reservoir rock. This implicates that the nanoparticles concentration, injection rate, salinity, and temperature do not affect their stability and the efficiency in porous media [24], because the polymeric nanoparticles will have the function of getting into the small pores, where crude oil remains trapped and modify the properties of reservoir fluids [12].

In this way, these systems could provide a viable alternative as a potential chemical injection fluid because their morphology, large surface area, active surfaces, chemical response, an improved viscosity and a favorable viscoelastic behavior [12, 25]. The viscosity behavior of injection fluid systems is an important factor, because it governs the displacement processes of material in oil reservoirs. Aqueous chemical fluids show a shear thinning or pseudoplastic flow behavior. This property is desirable to achieve the injectivity and oil mobilization control [12].

Currently for oil industry is important to determine and design the optimum concentrations of the injection fluids as well as an adequate understanding of the viscoelastic nature of injecting fluids [26, 27]. Particularly, the polymeric nanoparticles in emulsion show non-Newtonian behavior, shear thinning, non-zero elastic modulus and stress differences [28]. This means that viscosity and viscoelasticity of polymeric nanoparticles change with variations of shear rate [29]. Static and dynamic viscoelastic response of polymeric nanoparticles can be measured by rheological techniques. [30] In addition, viscoelastic behavior study provides knowledge about the dynamic moduli: storage or elastic modulus (G') and loss or viscous modulus (G'') changing some parameters such as temperature, surfactant concentration, salinity and nanoparticles concentration. [27] These rheological properties of nanoparticles are dictated by their microstructure. They depend on shear rate, surfactant, monomeric composition, concentration, temperature, reaction products, formation fluids and corrosion inhibitors [3, 31].

In this work, two systems of polymeric particles with possible applications in the matrix acidizing are proposed. Both particles have in their composition amino and carboxylic groups localized inside the particles in different way. The first one is core-shell polymeric particles where the core is composed by carboxylic groups, while the shell has amino groups. The second system is polymeric particles with a gradient of concentration where the interior is rich in carboxylic groups and poor of these groups in their surface while amino groups are reversed. The obtained materials were tested with calcium chloride and characterized by known techniques and the rheological and thermodynamic properties were measured. The results showed changes in their properties and the materials had conformational changes, when they interacted with Ca^{+2} ions because to the arrangements and concentrations of carboxylic groups inside the particles. This behavior could allow to control the reaction rate with the calcite rock and the formation of worm channels during the acid stimulation process.

Table 1 Information of chemical materials

Component	Source	CAS number	Molecular weight M_w/g·mol^{-1}	Mass fraction purity
Acrylic acid (AA)	Sigma-Aldrich, USA	79-10-7	72.06	≥ 98[a]
Acrylamide (AAm)	Sigma-Aldrich, China	79-06-1	71.08	≥ 98[a]
Methyl Methacrylate (MMA)	Poliformas Plásticas, Mexico	9002-93-1	100.13	≥ 90[a]
Sodium persulfate	Sigma-Aldrich, USA	7775-27-4	238.10	≥ 98[a]
IGEPAL CA-897	SOLVAY, USA	9002-93-1	–	–
Calcium chloride	Sigma-Aldrich, Japan	10043-52-4	110.98	≥ 97[a]
Destilled water	Mizu Técnica, Mexico	–	–	–

[a]Reagent grade

Table 2 Formulation 600 g of latex, ratio concentration 50:50 wt%: wt%

Component	Reactor (g)	Tank 1 (g)	Tank 2 (g)
Surfactant	0.0088	0.3745	0.3745
Methyl methacrylate (MMA)	–	5.4	5.4
Acrylic acid (AA)	–	3.6	–
Acrylamide (AAm)	–	–	3.6
Initiator	0.07	0.105	0.105
Desionized water	203.42	268.5	96.9

2 Experimental

2.1 Materials

Chemicals used in this work are summarized in Table 1. All reagents were used as received without further purification.

2.2 Synthesis of Polymeric Nanoparticles with Different Morphology

Two series of nanoparticles with different ratio concentrations of functional groups were synthesized. The materials were 100:0, 90:10, 80:20, 70:30, 60:40, 50:50, 40:60, 30:70, 20:80, 10:90 and 0:100 (wt%: wt%) acrylic acid (AA) and acrylamide (AAm), respectively. The reaction was carried out by emulsion polymerization techniques. The recipe used to prepare 600 g of latex with total functional groups of 40 wt% and a solids content of 3 wt% is shown in Table 2 as example.

Figure 1 shows a diagram of the synthesis process for both series. In Series 1, the addition was carried out in a semicontinuous process of two stages to obtain a core-shell morphology. In the stage 1 a pre-emulsion with acrylic acid was fed from Tank 1 to a reactor; while in the stage 2, a pre-emulsion with amide groups was fed from Tank 2 to the reactor. In Series 2 the synthesis was carried out by a power feed semicontinuous process. This process was used to generate a concentration gradient of acrylic acid and acrylamide

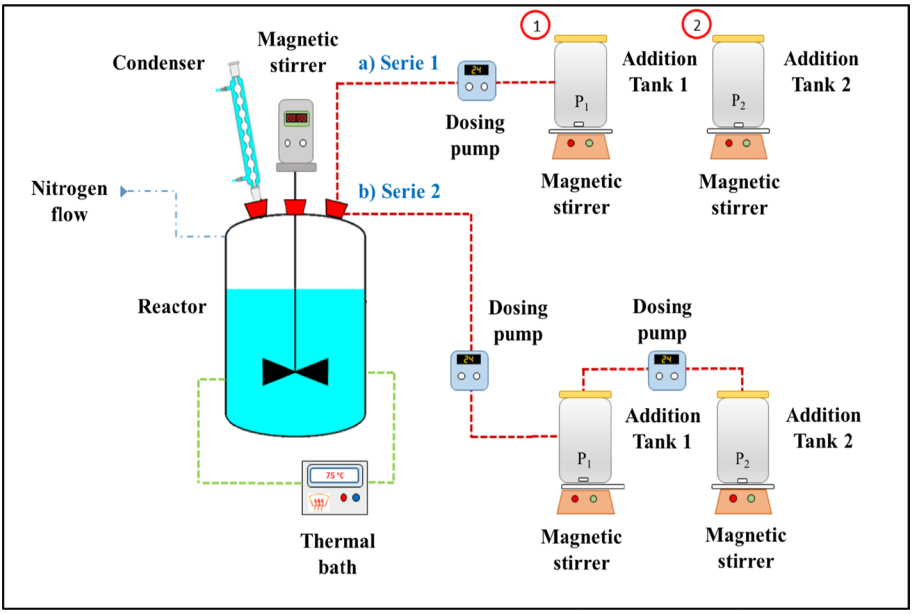

Fig. 1 Scheme of polymerization process of both series

inside polymeric particles. For that, two feeding tanks were connected in series to the reactor. A continuous pre-emulsion flow of acrylamide was fed from Tank 2 to Tank 1 (Fig. 1). Then, a continuous pre-emulsion flow of acrylic acid was fed from Tank 1 to the reactor. In both cases, two dosing pumps (ISMATEC, Wertheim, Germany) ensured the flow.

The synthesis process of latex used a 1 L glass reactor with a condenser under a dynamic flow of nitrogen. Temperature was maintained at 75 °C and controlled by a thermal bath (PolyScience temperature controller, Illinois, U.S.). A mechanical stirrer was used (HEIDOLPH, Schwabach, Alemania) and its rate was fixed at 250 rpm.

Figure 2 shows a scheme of two different obtained morphologies. Series 1 presents a highly concentration of carboxylic groups in the core and the amide groups are located

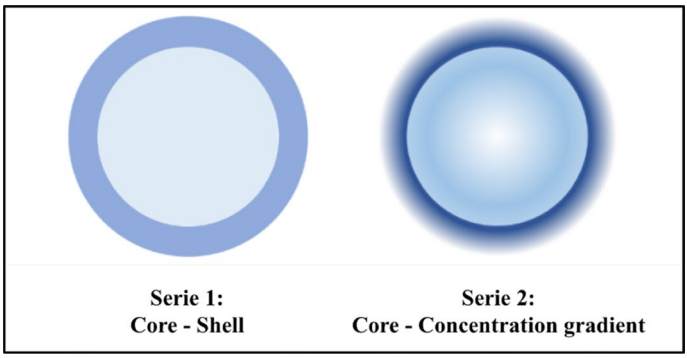

Fig. 2 Scheme of morphology of two series of polymeric particles. The color intensity indicates the concentration of carboxylic and amine groups

on the surface of polymeric particles. For Series 2, carboxylic and amide groups are located as a concentration gradient from the interior to the exterior of the particle.

2.3 Latex Characterization

2.3.1 Gravimetry

The total solid content for each material was calculated according to a method developed in previous works [32, 33].

2.3.2 Dynamic Light Scattering (DLS) and zeta Potential (ζ)

The particle diameter distribution and zeta potential (ζ) of the polymeric particles were measured using a Zetasizer Nano ZSP of Malvern Instruments, (Malvern, UK). The measurement protocol, calibration and operating conditions of this instrument have been described in detail elsewhere in the previous manual Malvern Instruments Zetasizer NANO [34]. The samples were diluted at 10 ppm with deionized water. The measurements were made by quadruplicate in a range from 25 °C to 60 °C.

From the particle size distribution, the average particle diameters were calculated using the following equations [32].

$$\overline{D_{\mathrm{z}}} = \frac{\sum n_i D_i^{\,5}}{\sum n_i D_i^{\,4}} \tag{1}$$

$$\overline{D_{\mathrm{n}}} = \frac{\sum n_i D_i}{\sum n_i} \tag{2}$$

$$\overline{D_{\mathrm{w}}} = \frac{\sum n_i D_i^{\,4}}{\sum n_i D_i^{\,3}} \tag{3}$$

The Polydispersity Index (*PDI*) was calculated using Eq. 1–3

$$PDI = \frac{D_{\mathrm{w}}}{D_{\mathrm{n}}} \tag{4}$$

where n_i is the number of particles, D_{z} is average hydrodynamic diameter, D_{n} is average diameter in number and D_{w} is average diameter in weight.

The colloidal stability changes of latex were measured by zeta potential. For that, the polymeric materials were diluted to a ratio of 1:10 latex- deionized water and 1 mL was put in a cell (DTS1070). The materials were titrated with an electrolyte, by means of a MULTI PURPOSE TITRATOR (MPT-2) from Malvern Instruments, (Malvern, UK). The measurements of zeta potential were carried out with an electrolyte concentration from 0 to 1.5 mol·L^{-1} at 25 °C.

2.3.3 Fourier Transform Infrared Spectroscopy (FT-IR)

The analysis of each latex was performed in an infrared spectrophotometer with ATR reflectance attenuator from Perkin Elmer model Frontier (Massachusetts, U.S.) with an energy of 236 E.U. The latex spectrum was measured in transmission mode over the middle region of the infrared spectrum between 4000–400 cm^{-1} at 30 °C.

2.3.4 Density and Sound Velocity

Density (ρ) and sound velocity (u) measurements were performed in a density and sound velocity meter DSA 5000 M from Anton Paar (Graz, Austria). The measurement protocol with a stated accuracy of ±0.1%, the calibration with high purity water and dry air and the operating condition of this instrument have been described in the instruction manual DSA 5000 M [35]. A titration cell was connected to the instrument, which is employed to change the concentration of the measured solution tomeasure. A degassed deionized water initially was placed in the cell free of air bubbles and a stock solution of latex was used as the titrant. Briefly, 12 injections of 8 mL of latex previously degassed by ultrasound for 20 min were performed. After each injection, the density (ρ) and sound velocity (u) of contained latex in the cell were measured. All measurements were carried out in a region of high dilution at $30 \leq T/°C \leq 60$. The changes in the latex concentration ($g{\cdot}mL^{-1}$) after each injection were calculated using the following equation [32, 36]:

$$C_{\mathrm{L}}^{i+1} = C_{\mathrm{L}}^{S} - \left(C_{\mathrm{L}}^{\mathrm{S}} - C_{\mathrm{L}}^{i}\right) e^{-\left(\frac{\Delta v}{V_{\mathrm{c}}}\right)} \tag{5}$$

where $C_{\mathrm{L}}^{\mathrm{S}}$ is the concentration stock of latex, C_{L}^{i} is the concentration of latex in the step i and C_{L}^{i+1} is the concentration of latex in step $i + 1$. The term Δv is the titration volume of latex stock solution and V_{C} is the cell volume.

2.3.5 Rheological Properties

The rheological properties of latex were measured using a Modular Compact Rheometer model MCR 502 from Anton Paar (Graz, Austria) in rotation mode. The measurement protocol, calibration and operation conditions of the rheometer before measurements have been described in detail in the instructions manual RheoCompass™ [37]. A sample of 18 mL of latex was deposited into the measurement system of concentric cylinder geometry (27 mm diameter). Measurements of viscosity were made at shear rate ($\dot{\gamma}$) from 0.01 to 100 s^{-1}. In other hand, a sample of 1 mL of latex was deposited onto rheometer base and the cone plate geometry (25 mm diameter, 1°) was collocated 1 mm above the base. Measurements of storage G' and loss G'' modulus were carried out a shear strain (γ) from 0.001 to 0.01, with an angular frequency (ω) of 1 s^{-1}. The measurements were carried out at $30 \leq T/°C \leq 60$.

2.3.6 Scanning Electron Microscopy (SEM)

The morphology of polymeric particles was observed in a JEOL JM-7800 F Field Scanning Electron Microscope equipment (Tokyo, Japan). Latex was diluted at ratio of 1:100 and deposited onto base of a cylindrical specimen holder with a diameter of 12 mm.

Latex titrated with electrolyte was not diluted for the analysis. The samples were dried with a visible light lamp at a 10 cm of distance from the sample. Before the analysis the polymeric materials were coated with a layer of gold. Finally, the samples were analyzed under the microscope with secondary electrons at accelerating voltage between 3.0 and 5.0 kV, a working distance (WD) from 4.0 to 10.0 mm and magnifications in the range from 10,000 to 50,000.

2.3.7 X'Ray Diffraction (DRX)

The diffractograms of the materials were obtained by an X-ray diffractometer from Rigaku model Miniflex 600, (Tokyo Japan). The diffraction angle 2θ was from 5 to 80°, the X-ray tube was made of Cu, the intensity of 15 mA and a voltage of 40 kV. The samples without titration and titrated with electrolyte were analyzed in powder at room temperature.

3 Results and Discussions

Two series of polymeric particles with different concentrations of monomers were obtained by means of emulsion polymerization techniques. All the obtained latex was used without further purification. Series 1 was synthesized with a core-shell morphology, while Series 2 was synthesized a core-gradient concentration morphology shown in Fig. 2. The total solids content for each series was determined using gravimetric techniques. The results show that total solids content of Serie 1 and 2 were close to 2 wt%.

The particle size distributions of polymeric materials with different morphologies were measured by dynamic light scattering (*DLS*) at 25 °C. The average hydrodynamic diameter of particles (D_z) was calculated from the obtained data and using the Eq. 1 while polydispersity index was calculated from Eq. 4, obtaining values close to 1.1.

Figure 3 shows D_z as a function of the AA concentration at several temperatures (T). It is observed for Series 1 (Fig. 3a) that if temperature increases, the average particle diameter decreases in all concentrations of AA except to the material with 20 wt% of AA, which does not present changes in size when the temperature changes. The polymeric material with 10 wt% of AA shows a significant decrement of diameter as temperature increases. This reduction of D_z can be explained because the particles have groups sensitive to temperature in their shell. These materials present a critical solution temperature at which they undergo phase transformations (see Fig. 4). As example, amide derivatives show a low-critical solution temperature (LCST) of ~ 32 °C; below it, they swell and above it, they contract [38, 39]. At $T >$ LCST, there is a break of hydrogen bonds between the polymeric chains and the water molecules. Here, the polymer-polymer hydrophobic interactions dominate and are thermodynamically favored [40, 41]. This behavior is attributed to the phase transition of the polymeric chains by the acrylamide present on the surface of particle. That is, the response of a thermo-sensitive polymer to stimuli is based upon thermodynamic principles. If the ΔG value of a polymer-solvent system at a certain temperature is positive, polymeric chains cannot be mixed into the solvent and two different phases of polymer and solvent will be formed separately. When, ΔG of thermo-responsive polymers at ambient temperature ($T <$ LCST) is negative, then the polymeric chains can be dissolved in an aqueous system, because water molecules form a thin layer around the hydrophilic portion of polymeric chains causing a negative value of ΔH in the process. Additionally, some water molecules interact by hydrogen bonding around hydrophobic

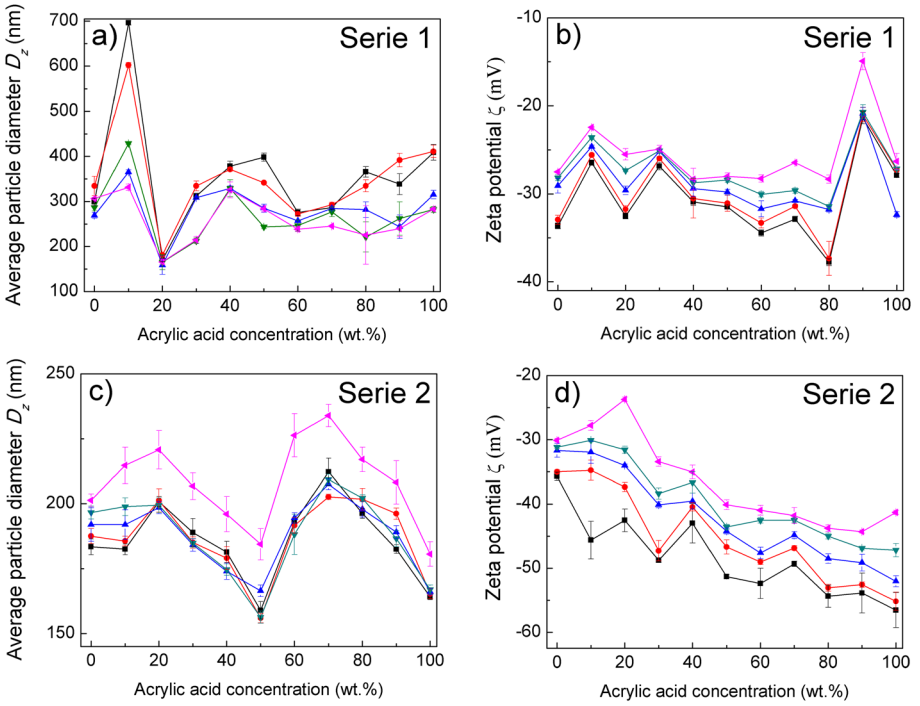

Fig. 3 Average diameter particle (D_z) and zeta potential (ζ) of **a** and **b** Series 1 and **c** and **d** Series 2 at: ■ 25 °C, ● 30 °C, ▲ 40 °C, ▼ 50 °C and ◀ 60 °C wt%: wt%. The uncertainties are around 10%

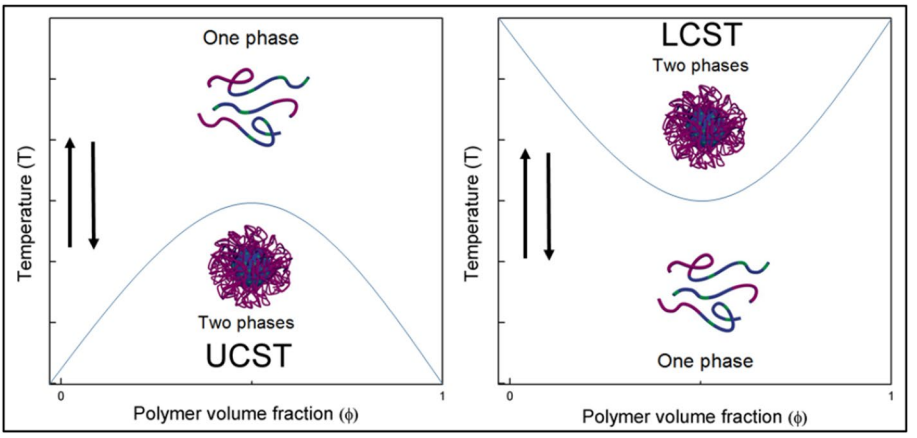

Fig. 4 Scheme of the upper critical solution temperature (UCST) and low critical solution temperature (LCST) of thermo-responsive polymers

segments and can lead to negative ΔS response. [42] This phenomenon occurs when the negative contribution of mixing enthalpy $\left(\Delta H_{\text{mix}} < 0\right)$ to the free energy of the systems is compensated by the entropic term$T\Delta S$, being the mixing entropy negative a consequence of

ordering $\left(\Delta S_{\mathrm{mix}} < 0\right)$ of polymeric chains [41]. However, when temperature increases above the critical point, ΔS of the system increases by breakage of the hydrogen bonding and decomposition of hydration layer. This means ΔH overcomes ΔS contributions, resulting in an unfavorable free energy of the system ($\Delta G > 0$) [42]. This behavior is accompanied by a collapse of the polymeric chains from elongated coils to collapsed globules. That is, D_z decreases as consequence of polymeric chains contraction [41].

Figure 3c presents the results of the change of D_z as a function of the AA at several temperatures for Series 2. The values of D_z are almost independent of temperature except at 60 °C, where its values increase abruptly. This behavior can be explained by the upper critical solution temperature (UCST) which is schematized in Fig. 4. Hydrogels prepared at this condition exhibit swelling with the increment of temperature. These materials are called positive thermosensitive gels [43]. A hydrogel of P(AA-co-AAm) with this arrangement in its functional groups is a system with a UCST behavior which is presented at ~ 25 °C. The UCST behavior is caused by interaction of hydrogen bonding between AA and AAm units and electrical repulsions of AA that form a polycomplex which is schematized in Fig. 5 [43–45]. These interactions can be broken upon heating of the system. This favors the diffusion coefficient of the polymeric chains and enhance their mobility [45]. In addition, the acrylic acid on the surface exhibits ionization, –COOH are dissociated to form $–COO^-$ groups. The osmotic pressure of the polymeric network and effect of electrostatic repulsive forces between $–COO^-$ produce swelling in the hydrogel [46].

The latex is swollen at temperatures above UCST by complex dissociation of P(AA-AAm) and the breakage of hydrogen bond as result, the D_z rises [47]. Therefore, the reduction of the diffusional motions of the polymeric chains at low temperature contribute to the formation of interactions between the amide groups and the carboxylic groups in the chains. [45, 48] This average size change of particle as a function of temperature can then be attributed to the volume phase transition temperature (VPTT) in both series [49].

The materials were also analyzed by zeta potential (ζ). It is related to the particle surface charge and the surface interaction with other molecules. The absolute value of zeta potential can be from zero to a hundred millivolts [50, 51]. However, a colloid is considered stable if the absolute value of ζ is equal or greater than the critical value of 30 mV [52], while ζ values of 5 mV reflect instability of colloidal systems with great tendency to agglomerate forming neutralized species [53].

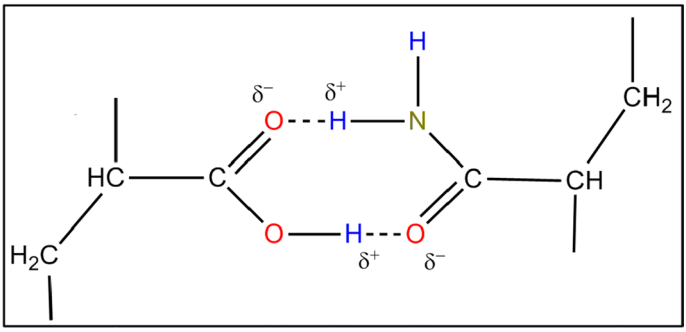

Fig. 5 Hydrogen bond interactions between the functional groups of acrylic acid and acrylamide

The zeta potential (ζ) data at different temperatures for Serie 1 are presented in Fig. 3b. The results show values $-15 < \zeta/\text{mV} < -40$ for all concentrations of AA and is observed the ζ increases as the temperature raises. Positively and negatively charged species are present in the P(AA-AAm) hydrogel particles. [53] For this reason, polymeric materials with a high content of AA have higher negative values of ζ because the great number of negatively charged of carboxyl groups [54]. If the values of ζ in the particle are negative, the repulsive electrostatic is the dominant force and tends to the stabilization of the emulsion but, if there is an increment in the values of ζ close to critical value, then van der Waals forces have an action of approaching and flocculating of the particles [55]. In addition, the presence of acrylamide on the surface of particles in Series 1 contributes with positive charges, increasing the ζ of particles. When the temperature increases, the high proportion of AAm on the surface also restricts the movement of carboxylic groups [53]. This is confirmed by the results obtained by FT-IR for all the series shown in Fig. 6. Thus, increasing the ionization of acid groups results in a proportional increment of ζ for a polymeric material dispersed in a medium [55]. When temperature raises, the kinetic energy of molecules also increases and the interactions between functional groups of material and water molecules weaken. Therefore, the van der Waals forces interactions are broken, and water molecules are moved out of the polymeric network.

The results of Series 2 present an increment of ζ as temperature increases and are shown in Fig. 3d. The obtained data show values $-59 < \zeta/\text{mV} < -36$ for all concentrations because the polymeric particles have a great concentration of carboxylic groups on the surface. The high amount of ionizable carboxylic groups on the surface gives higher values of ζ than Series 1. At high temperatures, the hydrogen bonds between the amide and carboxylic groups present in the polymeric chain are broken, causing particle swelling by an increment of the net change of carboxylic groups and then, the ζ increases.

The obtained materials were analyzed by FT-IR. Figure 6 presents spectra of materials with 100:0, 0:100 and 50:50 wt%: wt% AA-AAm for both series, as example. The spectrum of P(AA-co-AAm) confirms the formation of copolymer of acrylic acid and acrylamide.

The spectrum of the AA homopolymer is shown in Fig. 6a where the peaks of –OH groups appear at 3349 and 1100 cm^{-1} attributed to O–H of the carboxyl group [56]. The

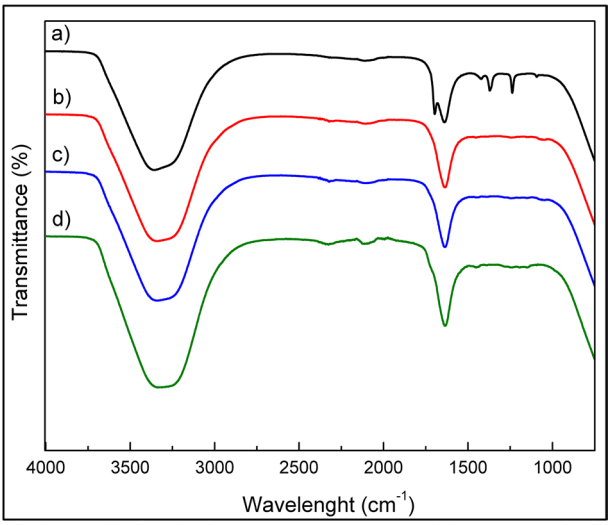

Fig. 6 FT-IR spectra of P(AA-co-AAm): (a) — 100:0, (b) — 0:100, (c) — 50:50 core-shell and (d) — 50:50 core-gradient wt%: wt% for Series 1 and Series 2

carbonyl stretching vibration C=O bonded to the carboxyl group –COOH appears as a peak between 1701 and 1630 cm^{-1} [57, 58]. The peaks between 1432, 1363, 1235 cm^{-1} are attributed to the C–O stretching vibration to –COOH [56].

Figure 6b shows the spectrum of AAm homopolymer, where the $–NH_{2}–$ stretching vibrational band is around 3328 cm^{-1}. Two bands appear at 2311 and 2112 cm^{-1} attributed to the presence of –CN group of the acrylamide [57]. The C=O band appears at 1639 cm^{-1} attributed to the amide. This band is generally overlapped with a second band assigned to $–NH_2$ vibrations [59]. Figure 6c and 6 d show the spectra of P(AA-co-AAm) core–shell and core-gradient, respectively.

There is a characteristic peak at 3322 cm^{-1} attributed to the stretching vibration of OH- and NH_2- associated to P(AA-co-AAm) [57, 59]. The characteristic band of $–NH_2$ in Fig. 6d becomes more intense than that of Fig. 6c. The peaks between 1630 and 1456 cm^{-1} represent the symmetric and asymmetric stretching of $–COO^-$ related at acrylic acid in the P(AA-co-AAm) spectrum [56, 57]. The formation of $–COO^-$ indicates the dissociation of carboxylic groups and the formation of complexes with the cationic groups of acrylamide through electrostatic interactions to form the copolymer during the polymerization process [57]. Infrared results indicate that the monomers were polymerized and the characteristic hydrophilic groups –COOH and $–CONH_2$ are still present without being affected during polymerization reaction for both series [60].

The materials were analyzed with a density and sound velocity meter. Supporting Information shows the experimental data of density and velocity of sound for both two series of polymeric particles at 30 °C, 40 and 60 °C. The specific volume and specific adiabatic compressibility as function of concentration is also shown in this file. From the obtained data, specific partial volume at infinite dilution ($v^0_{P;1}$) and specific partial adiabatic compressibility at infinite dilution ($k_S{}^0_{P;1}$) of polymeric particles at 30 °C, 40 and 60 °C were calculated using a methodology reported in previous works [36].

The partial volume can be broken down in the following contributions [36]:

$$v^0_{P;1} = v^0_{P;1/atom} + v^0_{P;1/free} + v^0_{P;1/hyd} \tag{6}$$

The term $v^0_{P;1/atom}$ represents the atomic volume of polymer chains. The term $v^0_{P;1/free}$ is the contribution that consider the empty space or free volume by the imperfect arrangement of polymeric chains inside the particle. The sum $v^0_{P;1/atom}+v^0_{P;1/free}$is the intrinsic contribution to the volume and is considered as the space where water molecules cannot penetrate. For this reason, the intrinsic volume is always positive. The $v^0_{P;1/hyd}$ is defined as the hydration term. This variable can be expressed as follow: [36]

$$v^0_{P;1/hyd} = n_h \left(v^0_{P;1/shell} - v_1 \right) \tag{7}$$

where $n_h$is the hydration number, $v^0_{P;1/shell}$ is the specific volume of the water molecules in the hydration shell and the v_1 is the specific volume in the bulk. The $v^0_{P;1/hyd}$ is a negative contribution to the intrinsic volume [36].

Figure 7a and b show the specific partial volume at infinite dilution $v^0_{P;1}$ as a function of concentrations of acrylic acid AA (wt%) for the Serie 1 and Serie 2, respectively. The Serie 1 shows an increment of $v^0_{P;1}$ in the range of concentration from 20 to 50 wt% of AA. This means, that there is a generation of free volume caused by electrostatic repulsions of functional groups into the polymeric particle. In terms of Eq. 6 is an increment of $v^0_{P;1/free}$ value. In addition, temperature increment causes the polymeric chains to be disentanglement and

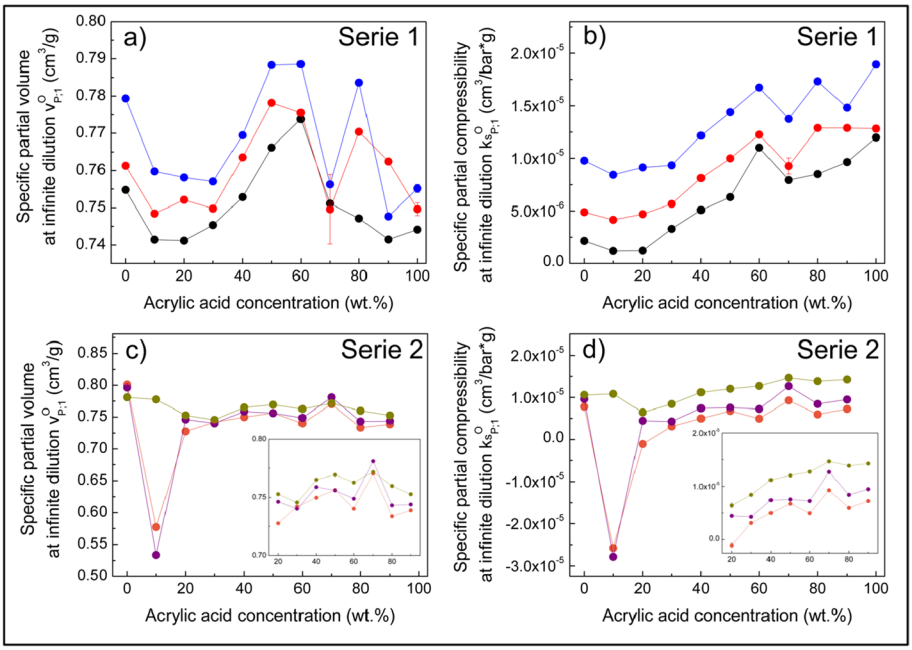

Fig. 7 Specific partial volume $\left(v^{0}_{P;1}\right)$ and compressibility $\left(k^{0}_{s_{P;1}}\right)$ at infinite dilution as a function of acrylic acid concentration AA (wt%): **a** and **b** Series 1 at ● 30 °C, ● 40 °C and ● 60 ºC and **c** and **d** Series 2 at ● 30 °C, ● 40 °C and ● 60 ºC. The uncertainties in the specific partial volume are of the order of 5×10^{-4} cm^3 g^{-1} and the uncertainties in the specific partial compressibilities are of the order of 10^{-6} cm^3 bar $^{-1}$ g^{-1}

then, there is an increment of $v^{0}_{P;1/free}$ and therefore, an increment of $v^{0}_{P;1}$. The highest values are reached between 50 and 60 wt% of AA. At high concentrations of AA (70, 80, 90 and 100 wt%), there is a decrement in the values of $v^{0}_{P;1}$ at 30 °C. This behavior can be explained using the Eq.6 where the increment of $v^{0}_{P;1/free}$ allows to entrance of a greater number of water molecules inside the particle, so the contribution of the $v^{0}_{P;1/hyd}$ is meaningful and thus, the values of $v^{0}_{P;1}$decreases; except for the proportion of 80 wt% of AA at 40 and 60 °C, where the $v^{0}_{P;1}$ rises.

In general, in Series 2, there are relevant changes with respect to the different proportions of AA when the temperature changes from 30 °C to 60 °C. The material with a concentration of 10 wt% of acrylic acid shows a drastic decrease of values of $v^{0}_{P;1}$. This is attributed to an increase of free volume contributions, because of the electrostatic repulsion of the carboxylic groups in the polymeric chains. Then the free volume is flooded by water molecules increasing the hydration contribution. This process is accompanying of average particle diameter increment [33]. In general, there is no change of $v^{0}_{P;1}$with temperature. This could be attributed to hydrogen bonding between the polymeric chains by the functional groups. These interactions were confirmed by FT-IR spectra. The repulsions between functional groups located on the surface induce some conformational changes in

the chains, causing cavities near surface of the particle, into which water molecules readily penetrate, leading to an increase in the hydration of the polymeric particle [36].

Comparing both series, they show a different behavior of the $v^0_{P;1}$ with respect to the composition and temperature. The location of the functional groups determines the hydration process of the polymeric particles. That means that the carboxylic groups located on the surface favor the increment of $v^0_{P;1/hyd}$ and therefore $v^0_{P;1}$ decreases. Now, if the carboxylic groups are located into the polymeric particle then steric hindrances impede conformational changes and hence the hydration of particle [36]. For this reason, the values of the $v^0_{P;1}$ from Series 2 are slightly lower than the values of $v^0_{P;1}$ of Series 1. This is, the particles of Series 2 are more hydrated than Series 1.

Similarly to volume, the specific partial compressibility ($k^0_{s_{P;1}}$) of a particle at infinite dilution is defined as [36]:

$$k^0_{s_{P;1}} = k^0_{s_{P;1/free}} + k^0_{s_{P;1/hyd}} \tag{8}$$

The atomic term does not appear in Eq. 8 due to the effect of the pressure on the atomic contribution $k^0_{P;1/atom}$ can be neglected. In fact, the van der Waals radii are essentially pressure independent because pressures up to several GPa do not affect the electron densities and covalent bond lengths [36].

The specific partial compressibility at infinite dilution $\left(k^0_{s_{P;1}}\right)$ as a function of acrylic acid concentration for Series 1 and Series 2 are shown in Fig. 7c and d, respectively. In the case of Series 1, the value of the compressibility $k^0_{s_{P;1}}$ increases with temperature. For concentrations between 0 and 20 wt% of AA the $k^0_{s_{P;1}}$ decreases similarly as specific partial volume, indicating a hydration process. Now, considering the obtained results in the D_z at these concentrations, it is possible that a swelling process inside the particle is going on.

There is another behavior of $k^0_{s_{P;1}}$ between 20 and 60 wt%, where the specific partial compressibility at infinite dilution increases with the AA concentration. In the same way, $v^0_{P;1}$ and D_z are increased in this concentration interval, indicating that an increment in the hydrodynamic diameter is produced by an increment of free volume contributions.

For concentrations between 70 and 100 wt% of AA the behavior of $k^0_{s_{P;1}}$ is more complicated. For example at 30 °C, there is an increase of $k^0_{s_{P;1}}$ indicating a free volume generation but there is a decrease of $v^0_{P;1}$, causing by an increase of hydration. All these effects are accompanied by an increase of D_z. This could be interpreted as a hydration process on the surface of particle and a free volume generation in the core that cause the increase of D_z. In the other hand, it is observed that when temperature increases, D_z decreases by the effect of the UCST, where the acrylamide groups are more hydrophobic and the non-covalent interactions are broken down. This explains the increase of $v^0_{P;1}$, and $k^0_{s_{P;1}}$.The behavior of $k^0_{s_{P;1}}$ for Series 2 is analogous to that of $v^0_{P;1}$. Comparing both morphologies, Series 1 is more compressible than Series 2 which can be attributed to the free volume generation in the core of polymeric particle.

Rheological properties at several temperatures were also measured for the synthesized latex. Figure 8 shows the viscosity (η) for latex with 90 wt% AA of Series 1 as an example, because all materials showed similar behavior. A decrease of viscosity (η) when the shear rate ($\dot{\gamma}$) increased is observed. This is attributed to the complex polymeric structure and deformation effects exhibited by the polymeric chains [55]. Latex has non-Newtonian behavior at low shear rate. When viscosity decreases, there is a

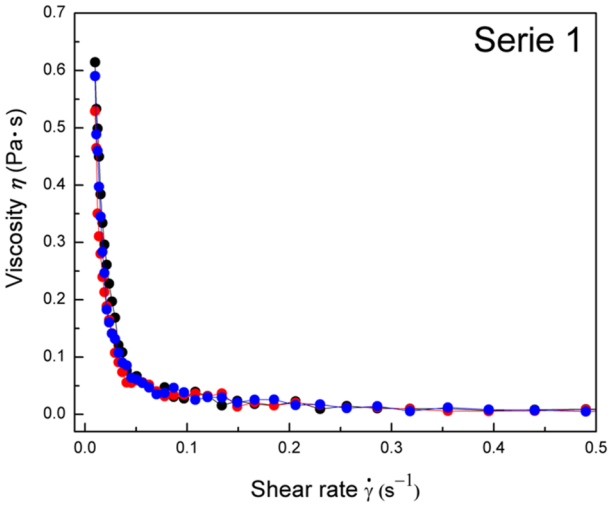

Fig. 8 Viscosity (η) as function of shear rate ($\dot{\gamma}$) of latex 90 AA wt% from Serie 1 at ● 30 °C, ● 50 °C and ● 60 °C. The uncertainties are around 10%

relationship between viscosity(η), shear stress (τ) and shear rate ($\dot{\gamma}$). This reduced viscosity also shows that latex is a pseudo-plastic material because its η decreases when $\dot{\gamma}$ is applied, by the gradual disentanglement of polymeric chains and their alignment in the direction of flow [61–63]. This means that the entangled polymeric chains are separated and stretched to be moved in the direction of the driving force [62]. When the shear rate increases above 0.5 s^{-1}, the viscosity becomes constant as if it was a Newtonian fluid. Under these conditions, the constant viscosity when stresses rise, indicating a hydrodynamic flow and these forces dominate [63]. This occurs when the polymeric chains are perfectly aligned in the direction of the applied force. In general, the studied nanoemulsions have viscosity values close to over the entire temperature range studied because they were synthetized as non-concentrated emulsions. For Series 2, the values of η are lower than for Series 1. This is due to that the particles of Series 2 swell at the studied temperatures and the polymeric chains have greater mobility and capacity to orient themselves in the direction of the applied stress.

Viscoelastic parameters of a material are relevant in the oil industry. For this reason, the storage (G') and loss (G'') modulus characterize the elastic and the viscous part of the viscoelastic behavior of a material. The G' values represent the stored energy, while G'' stands for the deformation energy that is lost by internal friction during shearing [64].

Viscoelastic properties were studied by measuring storage (G') and loss (G'') modulus as function of shear strain (γ) of latex. Figure 9 presents the results for the latex with 10 wt% of AA from Series 2 at 50 and 60 °C as an example, because Series 1 shows similar behavior. The results show that the G' increases rapidly and is higher than G'', indicating a more elastic response, i.e.solid-like behavior of the polymeric particle [64]. This is attributed to effect of swelling of the polymeric particle above their UCST as was described previously. As the D_z increases, the distance between the polymer particles decreases. It produces a greater particle-particle interaction and hence a higher resistance to flow. This enhancement in the viscoelastic behavior is related to the interconnected polymeric chains to create a continuous network when the temperature rises [65]. This means that the materials show a dilatant behavior where the viscosity

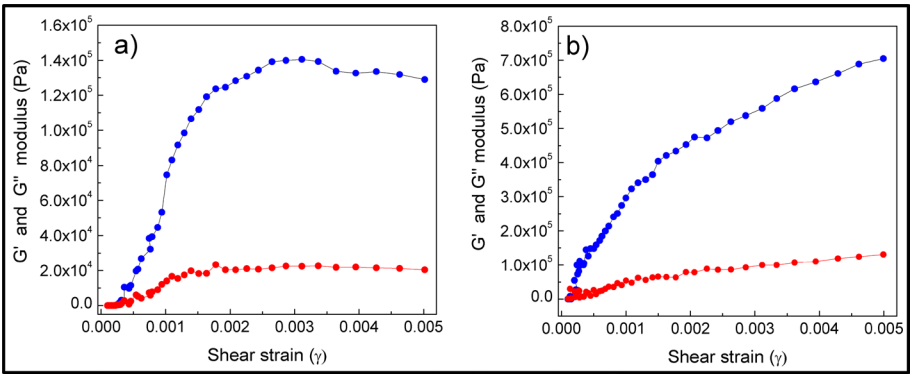

Fig. 9 ● Storage G' and ● loss G'' modulus as function of shear strain (γ) at **a** 50 °C and **b** 60 °C of latex with 10 wt% from Series 2. The uncertainties are around 10%

properties rise with increasing shear rate; thus, theses fluids are called shear thickening. On the other hand, at low shear rates the water lubricates the motion of each particle; the resulting stress is small. At high shear rates, the material expands or dilates slightly so that there is no longer sufficient water to fill the increased void space and prevents direct particle-particle contacts which result to an increment of friction and higher shear stress [66].

The stability of emulsions when they are in contact with the minerals present in the rock during the matrix acidification process is important for oil applications. For this reason, latex was analyzed by zeta potential when they were titrated with $CaCl_2$. Figure 10 shows the results of the latex 10:90 wt%: wt% from Series 2 as example. The ζ of nanoparticles without $CaCl_2$ is close to − 22 mV suggesting low colloidal stability. When the materials are put in contact with $CaCl_2$, the ζ is reduced to − 11 mV at 1.5 mol·L^{-1} of $CaCl_2$ without phase separation, because to the addition of the electrolyte screens the surface charges and decreases their stability. That is, the complex formed between carboxylic and amide groups is broken down by screen effect of Ca^{2+}, and as result two polymeric chains with

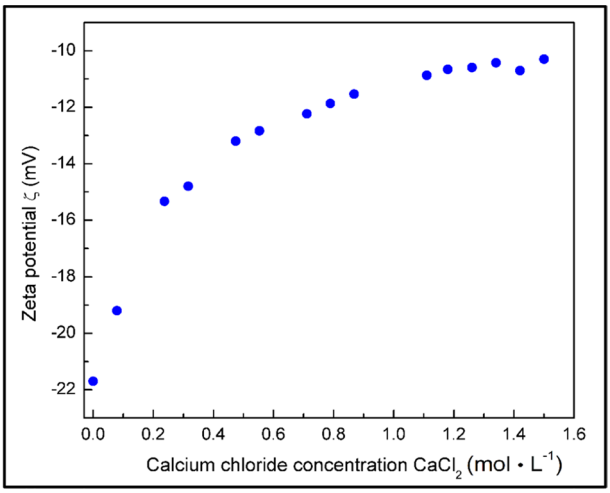

Fig. 10 Zeta potential (ζ) as function of calcium chloride ($CaCl_2$) concentration of latex 10:90 wt%: wt% from Series 2. The uncertainties are around 10%

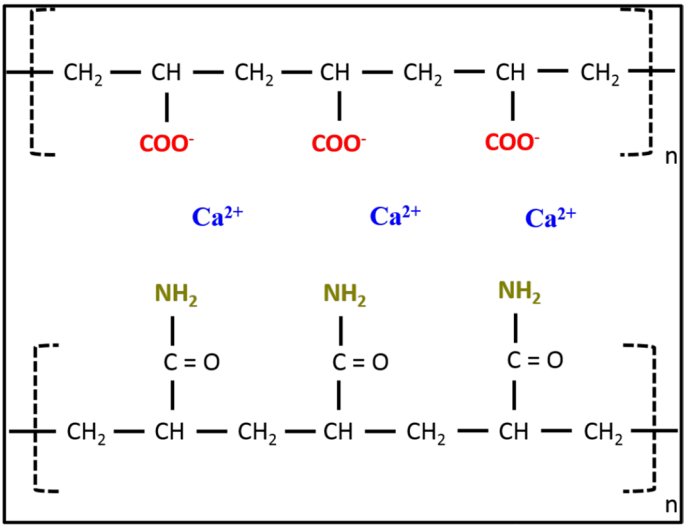

Fig. 11 Schematic illustration of the interaction between de carboxylic and amide groups and the calcium ion (Ca^{2+})

oppositely charged are formed (Fig. 11) [67]. In addition, the interaction between the carboxylate groups ions (COO^{-}) and the calcium ions (Ca^{2+}) result in an increment of ζ values. This behavior is observed in all latex for both series.

The morphology of the nanoparticles was observed by SEM. The nanoparticles without electrolyte of Series 1 and Series 2 are shown in Fig. 12a and b, respectively. The particles have a spherical morphology. When they were titrated with the electrolyte, an agglomeration of nanoparticles for Series 1 is presented in Fig. 12c. attributed to the loss of electrostatic repulsions between the groups of polymeric chain. This means an increment of zeta potential values from a high stability zone to an instability zone. In the case of Series 2 shown in Fig. 12d, the micrograph showed that the polymeric nanoparticles present a wafer-like morphology when they are in contact with the electrolyte. This behavior results from the disentanglement of the chains gave by the destruction of the formed interactions between the complex P(AA-co-AAm) and decrement of the colloidal stability of the system. That is, the chains are separated and tend to become more ordered. This is corroborated by the zeta potential data observed in Fig. 10.

The materials were also analyzed by XDR, when they were put in contact with the electrolyte. In general, the XRD spectra of P(AA-co-AAm) at 90:10 and 10:90 wt%: wt%. for Series 1 and Series 2 without titration are shown in Fig. 13a and b, respectively, as examples. The results showed a zone at $2\theta = 15.58°$ and $2\theta = 15.48°$ attributed to the amorphous polymeric structure and the characteristic peak to acrylic acid ($2\theta = 18.6°$) according to bibliography [68]. Two peaks of low intensity at $2\theta = 22.52°$ and 22.70° evidence a certain ordered structure by the polar role of acrylamide, while a broad zone around ~ 21° is evidence of an amorphous nature of AAm hydrogel network [69]. For P(AA-AAm) there is a wider diffraction zone in a range from $2\theta = 15°$ to 25° indicating an amorphous structure [69]. In conclusion, both series have a semicrystalline behavior attributed to the presence of hydrogen bonding within polymeric chains that are rising from –OH groups, which was corroborated by FT-IR [70].

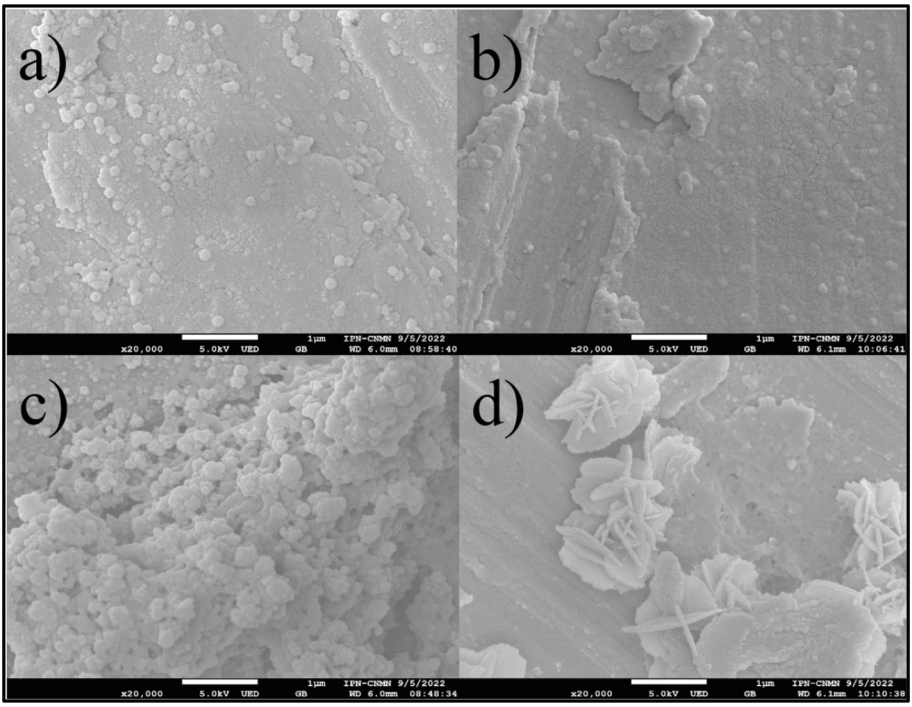

Fig. 12 Micrograph of P(AA-co-AAm) 10:90 wt%: wt% from **a** Series 1 and **b** Series 2: without titration and **c** Series 1 and **d** Series 2: titrated with calcium chloride ($CaCl_2$)

The results of XRD of polymeric particles interaction with electrolyte show structural changes in the particles (Fig. 13c and d). An increase in crystallinity is observed in both spectra. For latex with 90 wt% of AA of Series 1, the diffracted peaks are more intense than latex with 10 wt% of AA, which can be attributed to a greater quantity of $–COO^-$ groups which contribute to a greater interaction with Ca^{2+}. The same behavior is observed in the Series 2 when the latex was titrated with the electrolyte and a considerable increase in crystallinity was observed. The intensity of the diffracted peaks for both latex from Series 2 is more intense than those shown in Series 1, and can be attributed to the combination of functional groups producing the formation of the complex between AA and AAm. This favors the interaction with Ca^{2+}. Also, this was corroborated with the micrographs obtained by SEM for both series, where Series 1 presents an agglomeration, while Series 2 a structure more ordered forming wafer is observed.

4 Conclusions

Two series of smart polymeric materials were synthesized with a total solid content close to 2 wt%. The values of D_z showed that the conformational changes of the polymeric particles are dependent on their volume phase transition temperature (VPTT). The variation of temperature generates electrostatic repulsion of carboxylic groups and, the generation or breaking of weak interactions between the hydrophilic and hydrophobic parts of the

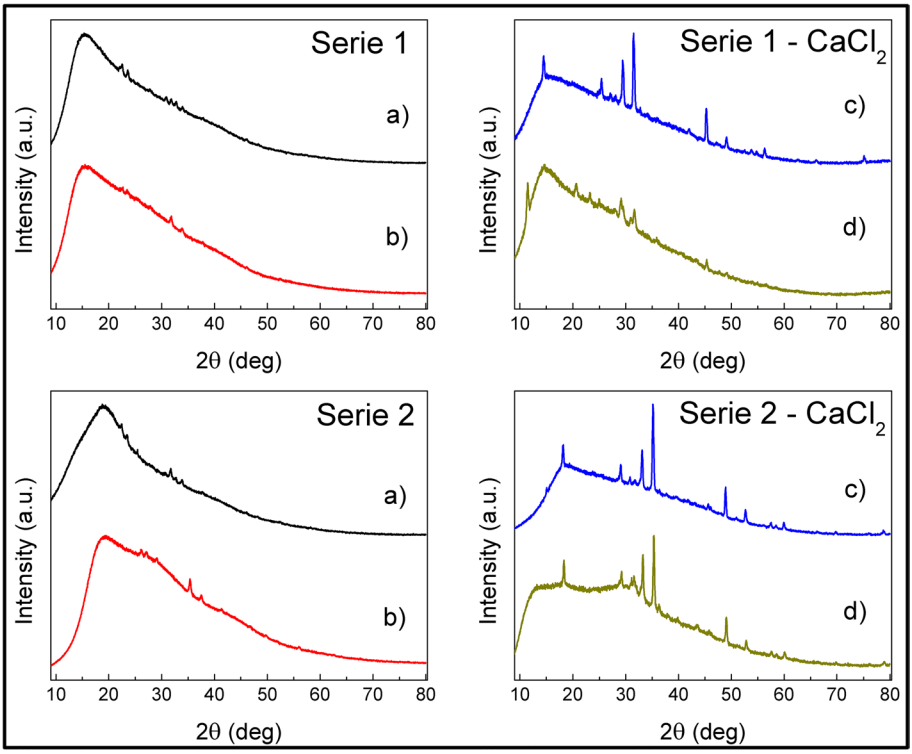

Fig. 13 XRD spectra of P(AA-co-AAm) wt%: wt%. from Series 1 and Series 2: (a) — 90:10, (b) — 10:90 without titration and (c) — 90:10 and (d) — 10:90 titrated with calcium chloride ($CaCl_2$)

polymeric chains and the water molecules. Moreover, zeta potential (ζ) values change as the proportions of AA and AAm are changed in the nanoparticles and increase with increasing temperature, which contributes to a decrease of the colloidal stability of latex. The analysis of the polymeric materials by FT-IR confirmed the formation of the copolymer of AA and AAm.

The specific thermodynamic properties of the polymeric materials are influenced by the proportions and location of the functional groups in the polymeric particles. In general, the behavior of specific partial volume ($v^0_{P;1}$) and specific partial adiabatic compressibility ($k^0_{s_{P;1}}$) at infinite dilution was attributed to the generation of electrostatic repulsions and the generation of free volume ($v^0_{P;1/free}$). At low concentrations of AA, the generation of $v^0_{P;1/free}$increased, while at high concentrations, the generated empty spaces contribute to an enhanced hydration process of the polymeric particle ($v^0_{P;1/hyd}$). In addition, temperature has an important effect on $v^0_{P;1}$ and $k^0_{s_{P;1}}$ values. This means that at higher temperatures the particle is more compressible. In the case of Series 1, the contraction of the particle when temperature increases contributes to the expulsion of water molecules from the polymeric chains causing an increase of the free volume. For Series 2, there are not some important changes of $v^0_{P;1}$ and $k^0_{s_{P;1}}$ with respect to temperature, because the formation of the complex P(AA-co-AAm) leads to the contraction or swelling of the particle.

Viscous properties showed a strong dependence on the applied stress. The polymeric materials were found to be non-Newtonian and to show pseudo-plastic behavior, as their viscosity (η) values decrease with increasing the shear rates ($\dot{\gamma}$) in both series. Thus, the applied stress causes the polymer-polymer interactions to break and allows the material to flow in the direction of the applied stress. Furthermore, the analysis of the viscoelastic properties shows a temperature dependence. Specifically, at 50 and 60°C there was an increase of the elastic modulus (G'), attributed to an increase in hydrophobic interactions between the polymeric chains in both series.

The obtained results for the studied polymeric materials when they were titrated with calcium chloride ($CaCl_2$) showed a strong interaction between the ionized carboxylic group (COO^-) and calcium ions (Ca^{2+}) corroborated by the obtained ζ values. The analysis by SEM showed spherical particles but when the polymeric material interacts with the calcium ions, an agglomeration of polymeric particles was observed for Series 1 and was reflected by the increment of ζ, while for Series 2 the micrographs showed that the polymeric chains unfold due to the loss of their interactions and to the decrement of their colloidal stability.

X-ray diffraction analysis showed a structure highly amorphous of latex before titration. When polymeric materials are titrated with the electrolyte, the crystallinity raised. This was attributed to the interactions between functional groups and calcium ions. Moreover, the higher amount of AA on the surface of the particle favored these interactions.

Supplementary Information The online version contains supplementary material available at https://doi.org/10.1007/s10953-023-01354-4.

Acknowledgements The authors express their gratitude to: CENTRO DE NANOCIENCIAS Y MICRO-NANOTECNOLOGIAS (CNMN IPN) CONACYT FOR THE SCHOLARSHIP GRANT ESCUELA SUPERIOR DE INGENIERÍA Y ARQUITECTURA (ESIA TICOMAN).

Author Contributions LRV: Experimental work, MAHM: Experimental work, GMM: Results analysis, RCB: Reologycal properties, JMdR: Write and review the paper, MC: Write and review the paper.

Declarations

Competing Interests The authors declare no competing interests.

References

1. Lv, Y.X., Wei, P., Zhu, X.H., Gan, Q., Li, H.B.: THMCD modeling of carbonate acidizing with HCl acid. J. Pet. Sci. Eng. **206**, 108940 (2021)
2. Mahmoud, M., Barri, A., Elkatatny, S.: Mixing chelating agents with seawater for acid stimulation treatments in carbonate reservoirs. J. Pet. Sci. Eng. **152**, 9–20 (2017)
3. Jia, C., Sepehrnoori, K., Huang, Z., Zhang, H., Yao, J.: Numerical studies and analysis on reactive flow in carbonate matrix acidizing. J. Pet. Sci. Eng. **201**, 108487 (2021)
4. Jafarpour, H., Aghaei, H., Litvin, V., Ashena, R.: Experimental optimization of a recently developed matrix acid stimulation technology in heterogeneous carbonate reservoirs. J. Pet. Sci. Eng. **196**, 108100 (2021)
5. Wang, L., Mou, J., Mo, S., Zhao, B., Liu, Z., Tian, X.: Modeling matrix acidizing in naturally fractured carbonate reservoirs. J. Pet. Sci. Eng. **186**, 106685 (2020)
6. Motta, A.B.G., Thompson, R.L., Favero, J.L., Dias, R.A.C., Silva, L.F.L.R., Costa, F.G., Schwalbert, M.P.: Rheological effects on the acidizing process in carbonate reservoirs. J. Pet. Sci. Eng. **207**, 109122 (2021)

7. Arji, A.H., Al-Azman, A., Le-Hussain, F., Regenauer-Lieb, K.: Acid stimulation in carbonates: A laboratory test of a wormhole model based on Damkohler and Péclet numbers. J. Pet. Sci. Eng. **203**, 108593 (2021)
8. Mustafa, A., Aly, M., Aljawad, M.S., Dvorkin, J., Solling, T., Sultan, A.: A green and efficient acid system for carbonate reservoir stimulation. J. Pet. Sci. Eng. **205**, 108974 (2021)
9. Garrouch, A.A., Jennings, A.R.: A contemporary approach to carbonate matrix acidizing. J. Pet. Sci. Eng. **158**, 129–143 (2017)
10. Liu, P., Li, J., Sun, S., Yao, J., Zhang, K.: Numerical investigation of carbonate acidizing with gelled acid using a coupled thermal hydrologic chemical model. Int. J. Therm. Sci. **160**, 106700 (2021)
11. Jafarpur, H., Moghadasi, J., Khormali, A., Petrakov, D.G., Ashena, R.: Increasing the stimulation efficiency of heterogeneous carbonate reservoirs by developing a multi-bached acid system. J. Pet. Sci. Eng. **172**, 50–59 (2019)
12. Pal, N., Mandal, A.: Enhanced oil recovery performance of Gemini surfactant-stabilized Nanoemulsion functionalized. Chem. Eng. Sci. **226**, 115887 (2020)
13. Onaizi, S.A.: Effect of salinity on the characteristics, pH-triggered demulsification and rheology of crude oil/water nanoemulsions. Sep. Purif. Technol. **281**, 119956 (2022)
14. Vatankhah, Z., Dehghani, E., Salami-Kalajahi, M., Roghani-Mamaqani, H.: Seed's morphology-induced core-shell composite particles by seeded emulsion polymerization for drug delivery. Colloids Surf. B. **191**, 111008 (2020)
15. Pakdel, P.M., Peighambardoust, S.J.: A review on acrylic based hydrogels and their applications in wastewater treatment. J. Environ. Manage. **217**, 123–143 (2018)
16. Qureshi, D., Nayak, S.K., Maji, S., Anis, A., Kim, D., Pal, K.: Environment sensitive hydrogels for drug delivery applications. Eur. Polym. J. **120**, 109220 (2019)
17. Al-Sakkaf, M.K., Onaizi, S.A.: Rheology, characteristics, stability, and pH-responsiveness of biosurfactant-stabilized crude oil/water nanoemulsions. Fuel. **307**, 121845 (2022)
18. Mu, M., Ebara, M.: Smart polymers. In Narain, R. (ed) Polymer Science and Nanotechnology. 1st edition, Elsevier, Alberta Canada, Chap. 12. (2020)
19. Lee, J., Badadagli, T.: Comprehensive review on heavy oil emulsions: Colloid science and practical applications. Chem. Eng. Sci. **228**, 115962 (2020)
20. Hajebi, S., Rabiee, N., Bagherzadeh, M., Ahmadi, S., Rabiee, M., Roghani-Mamaqani, H., Tahriri, M., Tayebi, L., Hamblin, M.R.: Stimulus-responsive polymeric nanogels as smart drug delivery systems. Acta Biomateralia. **92**, 1–18 (2019)
21. Shah, S., Rangaraj, N., Laxmikeshav, K., Sampathi, S.: Nanogels as drug carriers? Introduction, chemical aspects, release mechanisms and potential applications. Int. J. Pharm. **581**, 119268 (2020)
22. Bordat, A., Boissenot, T., Nicolas, J., Tsapis, N.: Thermoresponsive Polymer nanocarriers for biomedical applications. Adv. Drug Deliv Rev. **138**, 167–192 (2019)
23. Karakoc, O., Yegin, Y., Ozdogan, M., Salman, M., Nagabandi, N., Yegin, C., Yurukcu, M., Murat Sari, M.: In: Murat Sari, M., Temizel, C., Canbaz, C.H., Saputelli, L.A., Torsaeter, O. (eds.) Smart and State of the art Materials in oil and gas Industry. Sustainable Materials for Transitional and Alternative Energy, Elservier, (2021). Chap. 1
24. Abdelfatah, E., Pournik, M., Shiau, B.J.B., Harwell, J.: Mathematical modeling and simulation of nanoparticles transport in heterogeneous porous media. J. Nat. Gas Sci. Eng. **40**, 1–16 (2017)
25. Sircar, A., Rayavarapu, K., Bist, N., Yadav, K., Singh, S.: Applications of nanoparticles in enhanced oil recovery. J. Pet. Sci. Res. **7**, 77–90 (2021)
26. Gbadamosi, A.O., Junin, R., Manan, M.A., Yekeen, N., Agi, A., Oseh, J.O.: Recent advances and prospects in polymeric nanofluids application for enhanced oil recovery. J. Ind. Eng. Chem. **66**, 1–19 (2018)
27. Kumar, N., Mandal, A.: Oil in water nanoemulsion stabilized by polymeric surfactant: Characterization and properties evaluation for enhanced oil recovery. Eur. Polym. J. **109**, 265–276 (2018)
28. Perzzao, A., Tomaiuolo, G., Preziosi, V., Guido, S.: Emulsion in porous media: From single droplet behavior to applications for oil recovery. Adv. Colloid Interface Sci. **256**, 308–325 (2018)
29. Nair, R., Choudhury, A.R.: Synthesis and rheological characterization of a novel shear thinning levan gellan hydrogel. Int. J. Biol. Macromol. **159**, 922–930 (2020)
30. Vikram Singh Raghuwanshi, V.S., Garnier, G.: Characterization of hydrogels: Linking the nano to the microscale. Adv. Colloid Interface Sci. **274**, 102044 (2019)
31. Cheng, C.L., Hashemnejad, S.M., Zarket, B., Muthukrishnan, S., Doyle, P.S.: Thermally and pH-responsive gelation of nanoemulsions stabilized by weak acid surfactants. J. Colloid Interfce Sci. **563**, 229–240 (2020)
32. Santillán, R., Nieves, E., Corea, M., Río, D.: Synthesis of highly carboxylated latex particles using a power feed process. J. Ind. Eng. Chem. **19**, 1257–1266 (2013)

33. Pérez, A., Ruíz, A., Santillán, R., Río, D., Corea, J.M.: Partial volume and compressibility at infinite dilution of functionalized multilayer latex particles. React. Funct. **68**, 1422–1428 (2008)
34. Malvern Instruments.: Zetasizer nano user manual. In: Malvern Instruments (ed) Zetasizernano series user manual, p. pp. 1-11–13-11. Malvern Instruments Ltd, Malvern (2013)
35. Anton Paar.: Chap 11. Checking, adjusting and calibrating the instrument. In: Anton paar (ed) Instruction Manual DSA 5000 M. pp. 52–62. Anton Paar GmbH, Austria, (2011).
36. Santillán, R., Nieves, Alejandre, P., Pérez, E., Corea, E., Del, M., Río, J.M.: Comparative thermodynamic study of functional polymeric latex particles with different morphologies. Coll. And Surf. Phy Eng. Asp. **444**, 189–2098 (2014)
37. Paar, Anton: Chap 3. Setup. In: Paar, Anton (ed.) Instruction Manual Rheo Compass™ Software, pp. 19–40. Anton Paar GmbH, Austria (2011)
38. Hoogenboom, R.: Chap 2. Temperature responsive polymers: properties, synthesis, and applications. Smart polymers and their applications. In: Aguilar, M.R., San Román, J. (eds.) Smart Polymers and Their Application, 2nd edn, pp. 15–44. Woodhead Publishing, Cambridge (2014)
39. Patel, C.P., Parmar, V.K., Patel, P.S.: Stimuli-responsive polymers for ocular therapy. Stimuli Responsive Polymeric nanocarriers for Drug Delivery Applications. Adv. Ther. **2**, 463–489 (2019)
40. Pasparakis, G., Tsitsilianis, C.: LCST polymers: Thermoresponsive nanostructured assemblies towards bioapplications. Polymer. **211**, 123146 (2020)
41. Sponchioni, M., Palmiero, C.U., Moscatelli, D.: Thermo-responsive polymers: Aplicattions of smart materials in drug delivery and tissue engineering. Mat. Sc Eng. **102**, 589–605 (2019)
42. Mokhtariana, K., Masaeli, E.: Transiently thermally responsive surface: Concepts for cell sheet engineering. Eur. Pol. J. **141**, 110076 (2020)
43. Schmaljohann, D.: Thermo- and pH responsive polymers in drug delivery. Adv. Dru Del. R. **58**, 1655–1670 (2006)
44. Dilshad, Q., Suraj, Q.N., Samarendra, M., Arfat, A., Doman, K., Kunal, P.: Environment sensitive hydrogels for drug delivery applications. Eur. Pol. J. **120**, 109220 (2019)
45. Serrano, R.D., Alonso, C.P., Laurenti, M., Frick, B., Lopéz, E., Rubio, J.: Influence of the interchain hydrogen bonds on the thermoresponsive swelling behavior of UCST-like microgels. Polymer. **54**, 4963–4971 (2013)
46. Barbosa, J.A.C., Abdelsadig, M.S.E., Conway, B.R., Merchant, A.H.: Using zeta potential to study the ionization behaviour of polymers employed in modified-release dosage forms and estimating their pKa. Int. J. Pharm. **1**, 100024 (2019)
47. Xiao, X., Zhuo, R., Xu, J., Chen, L.: Effects of reaction temperature and reaction time on positive thermosensitivity of microspheres with poly(acrylamide)/poly(acrylic acid) IPN shells. Eur. Pol. J. **42**, 473–478 (2006)
48. Niskanen, J., Tenhu, H.: How to manipulate the upper critical solution temperature (UCST)? Polym. Chem. **8**, 220–232 (2017)
49. Ambreen, J., Sakhawat, H., Naemm, H., Ajmal, M.: Fabrication of poly (N-vinylcaprolactam-co-acrylic acid)-silver nanoparticles composite microgel with substantial potential of hydrogen peroxide sensing and catalyzing the reduction of water pollutants. J. Mol. Liq. **355**, 119–931 (2022)
50. Huang, G., Xu, B., Qiu, J., Peng, L., Luo, K., Liu, D., Han, P.: Symmetric electrophoretic light scattering for determination of the Zeta potential of colloidal systems. Coll. And Surf. Phy Eng. Asp. **587**, 124–339 (2020)
51. Dukhin, A.S., Xu, R.: Chap., : 3.2.5Zeta potential measurements. In: Hodoroaba, V.-D., Unger, W.E.S., Shard, A.G. (eds.) Micro and Nano Technologies, Measurements Processes for Nanoparticles, Characterization of Nanoparticles, 1st edn, pp. 213–224. Elsevier, New York (2020)
52. Ashrafizadeh, M., Tam, K.C.: Synthesis and physicochemical properties of dual-responsive acrylic acid/butyl acrylate cross-linked nanogel systems. J. Coll. Int. Sc. **556**, 313–323 (2019)
53. Mekewi, M.A., Madkour, T.M., Darwish, A.S., Hashish, Y.: Does poly(acrylic acid-co-acrylamide) hydrogel be the pluperfect choiceness in treatment of dyeing wastewater? "From simple copolymer to gigantic aqua-waste remover". J. Ind. Eng. Chem. **30**, 359–371 (2015)
54. Swilem, A.E., Elshazly, A.H.M., Hamed, A., Hegazy, E.A.: Nanoscale poly(acrylic acid)-based hydrogels prepared via a green single step approach for application as low-viscosity biomimetic fluid tears. Mat. Sc Eng. **110**, 110–726 (2020)
55. Fan, M., Nie, C., Du, H., Ni, J., Wang, B., Wang, X.: An insight into the solar demulsification of highly emulsified water produced from oilfields by monitoring the viscosity, zeta potential, particle size and rheology. Coll. And Surf. Phy Eng. Asp. **575**, 144–154 (2019)
56. Mistry, B.D.: Chap 2. Infrared spectroscopy. In: Mistry, B.D. (ed.) Handbook of Spectroscopy Data Chemistry (UV, IR, PMR, 13CNMR and Mass Spectroscopy), 1st edn, pp. 26–63. Oxford Book Company, Jaipur (2009)

57. Nesrinne, S., Djamel, A.: Synthesis, characterization and rheological behavior of pH sensitive poly(acrylamide-co-acrylic acid) hydrogels. A. J. Chem. **10**, 539–547 (2013)
58. Tang, H., Wei, F., Ding, H.: Transformation of the molecular structure of butyl methacrylate/acrylamide/acrylic acid copolymers during heat treatment. Mat. Des. **96**, 304–313 (2016)
59. Günzler, H., Gremlich, H.U.: IR spectroscopy and introduction. Clin. Chem. **49**, 1423 (2003)
60. Sun, N., Ji, R., Zhang, F., Song, X., Xie, A.: Structural evolution in poly(acrylic-co-acrylamide) pH-responsive hydrogels by low-field NMR. Mat. T Comm. **22**, 100748 (2019)
61. Ouarhim, W., Hassani, F.Z., Qaiss, A., Bouhfid, R.: Chap., : 5 Rheology of polymer nanocomposites. In: Thomas, S., Sarathchandran, C., Chandran, N. (eds.) Micro Nano technologies, Rheology of Polymer Blends and Nanocomposites. Theory, Modelling and Applications, 1st edn, pp. 73–96. Elsevier, New York (2020)
62. He, Y., Gou, S., Zhou, Y., Zhou, L., Tang, L., Liu, L., Fang, S.: Thermoresponsive behaviors of novel polyoxyethylene-functionalized acrylamide copolymers: Water solubility, rheological properties and surface activity. J. Mol. Liq. **319**, 114337 (2020)
63. Münstedt, H.: Chap 3. Characteristic properties of particles. In: Münstedt, H. (ed.) Rheological and Morphological Properties of Dispersed Polymeric Materials, 1st edn, pp. 39–50. Hanser publishing, Munich (2016)
64. Jastram, A., Claus, J., Janmey, P.A., Kragl, U.: Rheological properties of hydrogels based on ionic liquids. Polym. Test. **93**, 106943 (2021)
65. Domingues, S.C.J., Santos, R.R., Hubinger, M.D.: Thermo-rheological properties of chitosan hydrogels with hydroxypropyl methylcellulose and methylcellulose. Int. J. Bio Mac. **209**, 367–375 (2022)
66. Chhabra, R.P., Richardson, J.F.: Chap 1. Non. Newtonian fluid behaviour. In: Chhabra, R.P., Richardson, J.F. (eds.) Non-Newtonian Flow and Applied Rheology. Engineering Applications, 2nd edn, pp. 1–55. Butterworth-Heinermann, Oxford (2008)
67. Li, G., Zhang, G., Sun, R., Wong, C.P.: Dually pH-responsive polyelectrolyte complex hydrogel composed of polyacrylic acid and poly (2-(dimethylamino) ethyl methacrylate). Polymer. **107**, 332–340 (2016)
68. Tie, L., Ke, Y., Gong, Y., Zhang, W.X., Deng, Z.: Nanocellulose fine-tuned poly(acrylic acid) hydrogel for enhanced diclofenac removal. Int. J. Bio Mac. **213**, 1029–1036 (2022)
69. Jin, T., Xie, Z., Fullstone, D., Huang, C., Zeng, R., Bai, R.: Corrosion resistance of copolymerization of acrylamide and acrylic acid grafted graphene oxide composite coating on magnesium alloy. Prog Org. Coat. **139**, 105–222 (2019)
70. Rana, J., Goingi, G., Kaur, N., Kakati, K.S.: Synthesis and application of cellulose acetate-acrylic acid-acrylamide composite for removal of toxic methylene blue dye from aqueous solution. J. Water Process. Eng. **49**, 103–102 (2022)